JACS
JOURNAL OF THE AMERICAN CHEMICAL SOCIETY

Communication

pubs.acs.org/JACS

Aqueous CO_2 Reduction at Very Low Overpotential on Oxide-Derived Au Nanoparticles

Yihong Chen, Christina W. Li, and Matthew W. Kanan*

Department of Chemistry, Stanford University, 337 Campus Drive, Stanford, California 94305, United States

Supporting Information

ABSTRACT: Carbon dioxide reduction is an essential component of many prospective technologies for the renewable synthesis of carbon-containing fuels. Known catalysts for this reaction generally suffer from low energetic efficiency, poor product selectivity, and rapid deactivation. We show that the reduction of thick Au oxide films results in the formation of Au nanoparticles ("oxide-derived Au") that exhibit highly selective CO_2 reduction to CO in water at overpotentials as low as 140 mV and retain their activity for at least 8 h. Under identical conditions, polycrystalline Au electrodes and several other nanostructured Au electrodes prepared via alternative methods require at least 200 mV of additional overpotential to attain comparable CO_2 reduction activity and rapidly lose their activity. Electrokinetic studies indicate that the improved catalysis is linked to dramatically increased stabilization of the $CO_2^{\bullet-}$ intermediate on the surfaces of the oxide-derived Au electrodes.

Fossil fuels currently comprise >80% of global energy sources because of their availability, versatility, and high energy density. However, their continued use at this level will be accompanied by an unchecked accumulation of atmospheric CO_2. An attractive alternative is to develop a scalable synthesis of carbon-containing fuels using renewable energy, H_2O, and CO_2.[1−3] A key technological target for this goal is an efficient and robust electrochemical CO_2 reduction catalyst.[4,5] This catalyst could be used in an electrolyzer powered by a renewable electricity source or in a photoelectrochemical device that uses sunlight to power fuel synthesis directly.[6]

Electrochemical CO_2 reduction presents a host of challenges for catalyst development. An efficient catalyst must mediate multiple electron and proton transfers to CO_2 without resorting to excessive reducing potentials (overpotentials), reduce CO_2 in the presence of H_2O, and selectively produce one of many possible products. Efficient reduction of CO_2 to CO has been demonstrated at 700−900 °C in solid oxide electrolytic cells.[7,8] Overcoming the challenges of CO_2 reduction under mild conditions would enable development of a broader portfolio of fuel-producing devices. To this end, researchers have evaluated most polycrystalline metals as electrodes for room-temperature CO_2 reduction in aqueous solutions.[9] While several polycrystalline metals are competent for CO_2 reduction under these conditions, all suffer from one or more of the following problems: low energetic efficiency (i.e., high overpotential requirement), poor selectivity, and rapid loss of CO_2 reduction activity in favor of H_2O reduction.[10−12]

Researchers have previously attempted to enhance the activity of polycrystalline metals by using an ionic liquid electrolyte to stabilize the putative $CO_2^{\bullet-}$ intermediate of CO_2 reduction,[13] embedding metal particles in a cationic polymer,[14] or using pyridine as a soluble catalyst.[15,16] While these approaches have achieved significant reductions in overpotential, they have thus far been limited to low current densities. Moreover, use of ionic liquids, pyridine, or other additives to the electrolyte may prove problematic for long-term operation of an electrolyzer. Developing an efficient and robust catalyst that operates in cells requiring only H_2O and CO_2 as inputs remains a major obstacle to the advancement of CO_2 fixation technology.

The poor performance of polycrystalline metal electrodes indicates that efficient CO_2 reduction requires either use of alternative materials or preparation of metal particles with catalytically active surface structures that are distinct from those that dominate the polycrystalline surfaces. We recently discovered that Cu nanoparticle (NP) films prepared by electrochemically reducing thermally grown Cu_2O layers exhibit dramatically improved selectivity for CO_2 vs H_2O reduction at low overpotential and high resistance to deactivation relative to polycrystalline Cu electrodes.[17] Activities of Cu NP films were correlated with precursor Cu_2O layer thickness: >1 μm of Cu_2O was required for large improvements in activity. As a result, we hypothesized that reduction of thick metal oxide layers could be a general route to accessing metal NP catalysts with improved CO_2 reduction activity.

Gold was targeted as an electrode material because it is reported to exhibit the highest activity and selectivity for CO_2 reduction to CO among polycrystalline metals.[9,18] Thermal oxidation of Au, however, is prohibited because Au oxide (Au_2O_3) decomposes above 160 °C.[19] We thus turned to electrochemical methods to oxidize Au electrodes. Constant potential anodization was only effective for forming very thin oxide layers that were reduced within seconds upon application of a cathodic potential. In contrast, thick (>1 μm), amorphous Au oxide layers were prepared on Au electrodes by applying a periodic symmetric square-wave potential routine at 1 kHz in 0.5 M H_2SO_4 (see Supporting Information (SI) and Figure S1).[20] The resulting electrodes were used directly in CO_2 reduction electrolyses performed in $NaHCO_3$ electrolytes, during which oxide was reduced to Au^0 within 15 min.

Received: September 20, 2012
Published: November 21, 2012

   dx.doi.org/10.1021/ja309317u | J. Am. Chem. Soc. 2012, 134, 19969−19972

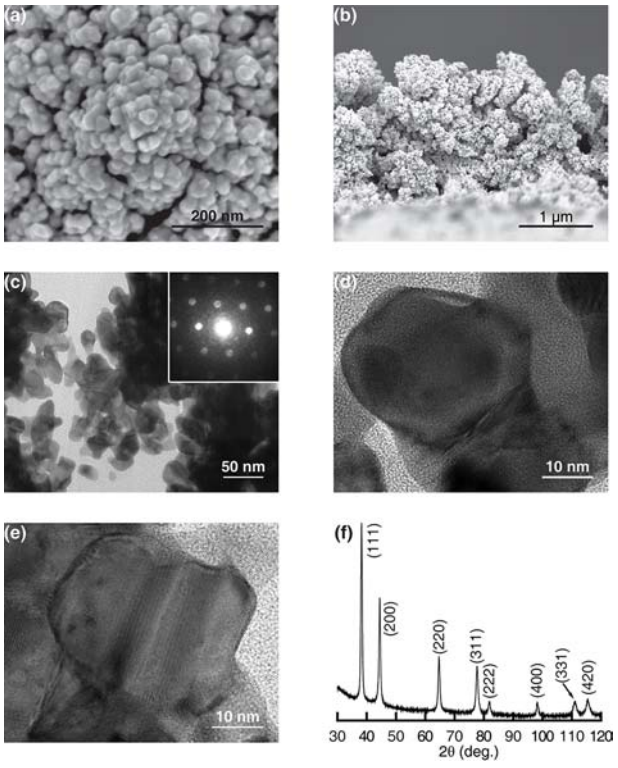

Figure 1. Characterization of oxide-derived Au NPs. (a) Top-down and (b) cross-sectional SEM images, (c) low-magnification TEM image and nanobeam electron diffraction pattern (inset), (d,e) high-magnification TEM images, and (f) PXRD pattern.

Figure 1 shows electron microscopy and diffraction data for the reduced electrodes ("oxide-derived Au"). SEM images indicated that the electrodes were comprised of 1−2 μm thick films of agglomerated Au NPs with particle sizes of ∼20−40 nm (Figure 1a,b). Similar particle sizes were also observed by low-resolution TEM (Figure 1c), and high-resolution TEM indicated that the particles were single Au crystallites (Figure 1d,e). Single-crystal diffraction patterns were observed by nanobeam electron diffraction (Figure 1c, inset). Consistent with these results, PXRD exhibited the expected peaks for a metallic Au lattice (Figure 1f), and average crystallite size determined by line broadening analysis was 23 ± 6 nm (Figure S2). Finally, XPS and EDXS exhibited the expected peaks for Au^0 and no peaks attributable to an oxide, indicating that reduction of Au_2O_3 was complete within the detection limits of these techniques (Figure S2).

CO_2 reduction activities of oxide-derived Au and polycrystalline Au electrodes were determined by performing constant-potential electrolyses in CO_2-saturated 0.5 M $NaHCO_3$, pH 7.2. Oxide-derived Au electrodes were formed in situ via reduction of the precursor Au oxide-coated electrodes in the initial period of the electrolysis. Electrolyses were performed in two-compartment cells, and headspace of the cathodic compartment was continuously purged with CO_2 into the sampling loop of a GC, enabling quantification of gas-phase products every 15 min. Samples of cathodic electrolyte were removed at the end of the electrolyses and analyzed by ^{1}H NMR to quantify solution-phase products.

Figure 2a shows total geometric current density (j_{tot}) vs time and Faradaic efficiency (FE) for CO vs time for polycrystalline Au and oxide-derived Au electrodes at −0.4 V vs reversible hydrogen electrode (RHE; all potentials reported here are with respect to this reference). Since the CO_2/CO equilibrium potential is −0.11 V vs RHE,[21] −0.4 V corresponds to 0.29 V of overpotential for CO production (η_{CO}). Oxide-derived Au exhibited an initial j_{tot} of ∼40 mA/cm^2 that rapidly declined to ∼10 mA/cm^2 in the first 10 min of electrolysis during which reduction of the Au oxide layer took place. Thereafter, j_{tot} declined much more slowly, reaching 6 mA/cm^2 after 8 h. During this period, FE for CO production was nearly quantitative (>98%). In contrast, polycrystalline Au exhibited a j_{tot} that declined from an initial value of 0.5 mA/cm^2 to <20 μA/cm^2 over 1 h of electrolysis and slowly declined to <10 μA/cm^2 over the remaining 7 h. The FE for CO was ∼40% in the first hour but dropped to <5% over the next 2 h. The remainder of the current was accounted for by H_2 evolution.

To compare the activities per unit area of Au surface for polycrystalline and oxide-derived Au, surface areas for the two electrodes were determined by measuring anodic stripping waves for under-potential deposited (upd) Cu monolayers (see SI).[22] A roughness factor (RF) of 72 was obtained for an oxide-derived Au electrode analyzed after 15 min of electrolysis at −0.4 V, which is just long enough for complete reduction of the precursor Au oxide layer. After 8 h, however, the RF was reduced to 17, indicating that sintering of Au NPs occurred during CO_2 reduction electrolysis. SEM and PXRD line-broadening analysis of these electrodes after 8 h showed an increase in particle and crystallite size over time, consistent with the observed RF decrease (Figures S2 and S3). This sintering most likely accounts for the slow reduction in j_{tot} observed for oxide-derived Au after the initial Au oxide reduction period but does not affect the selectivity for CO_2 reduction. Change in RF for oxide-derived Au and rapid decline in j_{tot} for polycrystalline Au make it difficult to

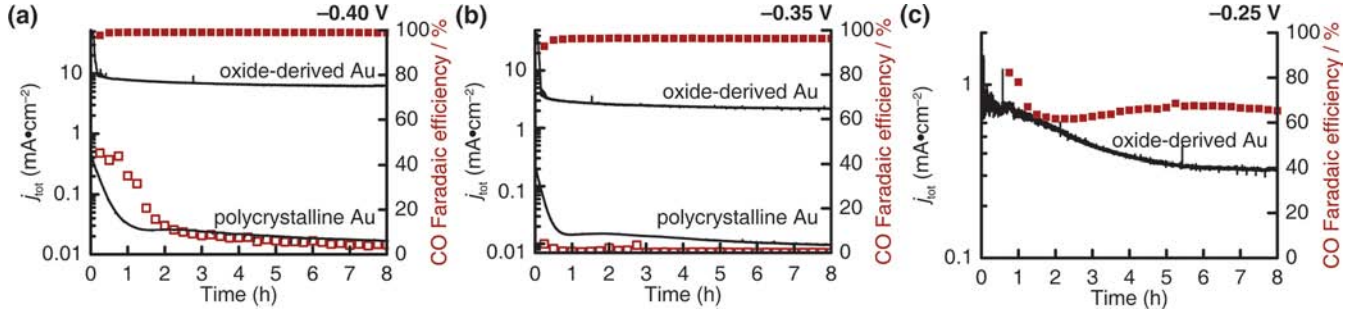

Figure 2. Comparison of CO_2 reduction activity of polycrystalline Au with that of oxide-derived Au. Total current density vs time (—, left axis) and FE for CO production vs time (right axis) on oxide-derived Au (red, ■) and polycrystalline Au (red, □) in electrolyses at (a) −0.4, (b) −0.35, and (c) −0.25 V vs RHE. Data were obtained in CO_2-saturated 0.5 M $NaHCO_3$, pH 7.2.

dx.doi.org/10.1021/ja309317u | J. Am. Chem. Soc. 2012, 134, 19969−19972

quantitatively compare surface area-normalized activities for the two electrodes. Nonetheless, even the initial RF of 72 is significantly smaller than the differences in j_{tot} over the course of electrolyses, indicating a substantial enhancement in normalized current density for oxide-derived Au, in addition to a change in selectivity for CO_2 vs H_2O reduction.

Greater differences in CO_2 reduction activity between oxide-derived and polycrystalline Au were observed at lower overpotentials. At −0.35 V (η_{CO} = 0.24 V), oxide-derived Au electrodes exhibited j_{tot} = 2−4 mA/cm^2 over the course of an 8 h electrolysis and >96% FE for CO (Figure 2b). In contrast, polycrystalline Au exhibited very low current densities (<20 μA/cm^2) and nearly exclusive H_2 evolution at this potential, FE for CO declining from 1−4% in the first hour to a nearly undetectable level for the remainder of the electrolysis. No significant CO_2 reduction was observed for polycrystalline Au above −0.35 V, whereas oxide-derived Au continued to reduce CO_2 with high FE at considerably lower overpotentials. At −0.25 V (η_{CO} = 0.14 V), oxide-derived Au exhibited j_{tot} = 0.3−0.5 mA/cm^2 with a FE of 65% for CO (Figure 2c). HCO_2^- formation was also observed, corresponding to a FE of 11%, while the remainder of the current was accounted for by H_2 evolution. Similar reductions in RFs were observed for oxide-derived Au electrodes used in electrolyses at these more positive potentials to that observed at −0.4 V, accounting for slow reductions in j_{tot} values. CO_2 reduction FEs at various potentials between −0.2 and −0.5 V for polycrystalline Au and oxide-derived Au electrodes are summarized in Figure 3. Values for polycrystalline Au are averages over the first 40−60 min of electrolysis because of rapid loss of CO_2 reduction observed for this electrode.

Several other modified Au electrodes were evaluated in CO_2 reduction electrolyses to assess the uniqueness of the activity of oxide-derived Au NPs. Constant potential anodization of a polycrystalline Au electrode in 0.5 M Na_2HPO_4 for 2 days resulted in a thin oxide layer that was reduced within seconds upon application of a cathodic potential.[23] CO_2 reduction activity of the reduced electrode was initially enhanced relative to polycrystalline Au but decayed precipitously within 2 h (Figure S5). A high surface area nanoporous Au electrode was prepared by anodization of a Au electrode in aqueous oxalic acid.[24] This electrode exhibited increased initial FEs for CO relative to polycrystalline Au but rapidly lost its CO_2 reduction activity within 1−2 h (Figure S6). Electrodes prepared from commercially available 15 nm Au NPs exhibited increased surface area and j_{tot} relative to polycrystalline Au but no enhancement in FE for CO_2 reduction and a similar loss of activity after 2 h of electrolysis (Figure S7). A previous evaluation of electrodes comprised of 2 and 5 nm Au NPs obtained minimal CO_2 reduction activity above −0.5 V.[25] Together, results indicate that simply increasing surface area of a Au electrode or forming nanoscale structural features is not sufficient to substantially improve CO_2 reduction properties.

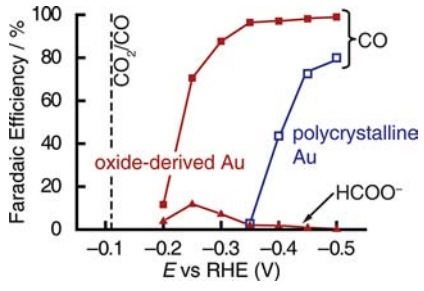

Figure 3. FEs for CO and HCO_2^- production on oxide-derived Au and polycrystalline Au electrodes at various potentials between −0.2 and −0.5 V in 0.5 M $NaHCO_3$, pH 7.2. Dashed line indicates the CO equilibrium potential.

To investigate the importance of morphology to the CO_2 reduction activity, an oxide-derived Au electrode was annealed at 140 °C under vacuum prior to electrolysis. While the annealing process had little effect on the electrode morphology and crystallite size as determined by SEM and PXRD, the annealed electrode exhibited very low FE for CO_2 reduction despite similar j_{tot} values to an unannealed sample (Figure S8). Maintenance of the overall electrode morphology but the loss of CO_2 reduction activity resulting from the annealing process suggests that activity of oxide-derived Au is linked to unique metastable structures that are formed on particle surfaces during reduction of the thick oxide precursor.

Stable CO_2 reduction efficiency on oxide-derived Au electrodes enabled the obtainment of electrokinetic data to probe the mechanism of CO_2 reduction to CO. Partial current density for CO production (j_{CO}) as a function of potential was extracted from data for the constant potential electrolyses. A plot of $\log(j_{CO})$ vs η (Tafel plot) exhibits a slope of 56 mV/dec from j_{CO} = 0.02 to 2 mA/cm^2 and curves to 180 mV/dec for larger values of j_{CO} (Figure 4a). Upward Tafel slope curvature at high current density likely reflects mass transport limitations in this regime. The 56 mV/dec slope in the low current density regime is indicative of a 1 e^- pre-equilibrium prior to a rate-determining chemical step (i.e., one that does not involve e^- transfer).[26,27] To determine the reaction order with respect to HCO_3^-, electrolyses were performed at a constant applied potential at HCO_3^- concentrations ranging from 1.0 to 0.1 M, with $NaClO_4$ added to the electrolyte to maintain ionic strength. A plot of $\log(j_{CO})$ vs $\log([HCO_3^-])$ exhibits a slope of 0.96, indicating approximate first-order dependence of the reaction rate on HCO_3^- (Figure 4b). Finally, dependence of j_{CO} on partial pressure of CO_2 was measured at constant potential. A plot of $\log(j_{CO})$ vs $\log(p_{CO_2})$ exhibits a slope of 0.92, indicating approximate first-order dependence on concentration of CO_2 in solution (Figure 4c).

Obtainment of analogous electrokinetic data for polycrystalline Au was hindered by the relatively rapid loss of CO_2 reduction activity observed for this electrode under identical conditions. Nonetheless, j_{CO} data for polycrystalline Au in the first hour of electrolysis indicate a 114 mV/dec Tafel slope, much higher than observed for oxide-derived Au. Previous electrokinetic studies on polycrystalline Au in bicarbonate electrolyte and phosphate buffer yielded Tafel slopes of 148 and 129 mV/dec, respectively, which are consistent with data obtained in this work (Figure S9).[18,28]

Tafel slopes on polycrystalline Au indicate a rate-determining initial e^- transfer to CO_2 to form an adsorbed $CO_2^{\bullet-}$ intermediate. The overpotential required for this step is typically large on polycrystalline metal electrodes due to poor stabilization of $CO_2^{\bullet-}$ by the metal surface. In contrast, electrokinetic data for oxide-derived Au support a mechanism that involves a reversible e^- transfer to CO_2 to form adsorbed $CO_2^{\bullet-}$ followed by a rate-determining H^+ transfer with HCO_3^- serving as the H^+ donor. Subsequent relatively fast steps involving additional e^- and H^+ transfers complete the reduction to CO (Scheme 1). Mechanistic divergence from rate-determining 1e^- transfer suggests that active sites on the surfaces of oxide-derived Au NPs provide better stabilization for $CO_2^{\bullet-}$ than the sites on polycrystalline Au.

dx.doi.org/10.1021/ja309317u | J. Am. Chem. Soc. 2012, 134, 19969−19972

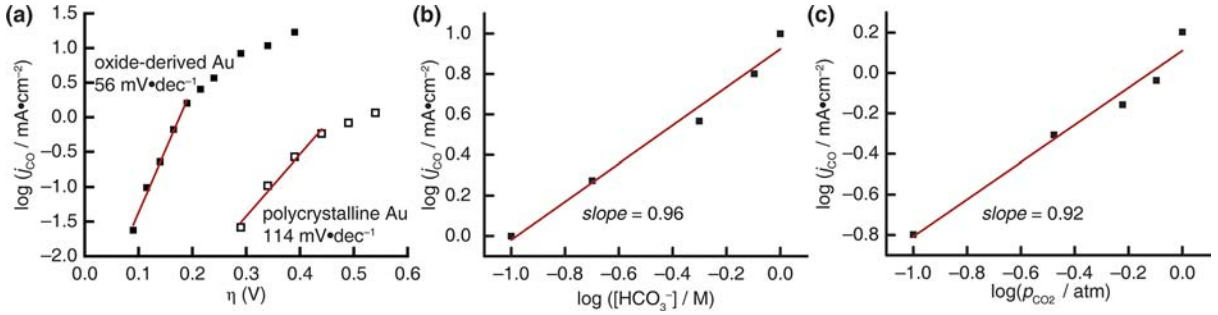

Figure 4. Electrokinetics of CO_2 reduction to CO on oxide-derived Au. CO production partial current density vs (a) potential on oxide-derived Au and polycrystalline Au, (b) sodium bicarbonate concentration at constant potential, and (c) CO_2 partial pressure at constant potential.

Scheme 1. Proposed Mechanisms for CO_2 Reduction to CO on Polycrystalline Au and Oxide-Derived Au

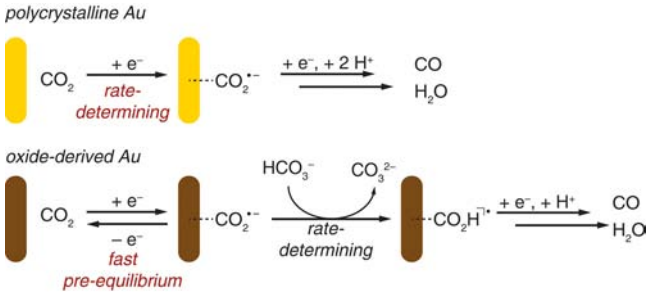

Collectively, our results indicate that Au oxide reduction results in Au particles with metastable surfaces that accelerate CO_2 reduction catalysis. Exceptional activity of these catalysts indicated by their low Tafel slopes, high exchange current densities, and resistance to deactivation demonstrates that energetically efficient CO_2 fixation at useful rates is possible without resorting to extreme conditions. Future efforts to elucidate atomic-level structural information about the surfaces of oxide-derived Au may provide key structure−activity insights for efficient CO_2 reduction that are not obtainable from studies of less active catalysts. More broadly, we anticipate that other highly active CO_2 reduction catalysts will emerge from an extensive exploration of metal structures beyond polycrystalline and single crystalline electrodes.

■ ASSOCIATED CONTENT

Supporting Information

Experimental procedures and additional data. This material is available free of charge via the Internet at http://pubs.acs.org.

■ AUTHOR INFORMATION

Corresponding Author

mkanan@stanford.edu

Notes

The authors declare no competing financial interest.

■ ACKNOWLEDGMENTS

We thank Stanford University and the Precourt Institute for Energy (PIE 10-008) for support of this work. C.W.L. acknowledges a NSF Predoctoral Fellowship.

■ REFERENCES

(1) Olah, G. A.; Prakash, G. K. S.; Goeppert, A. *J. Am. Chem. Soc.* **2011**, *133*, 12881.
(2) Arakawa, H.; et al. *Chem. Rev.* **2001**, *101*, 953.
(3) Graves, C.; Ebbesen, S. D.; Mogensen, M.; Lackner, K. S. *Renewable Sustainable Energy Rev.* **2011**, *15*, 1.
(4) Bell, A. T.; Gates, B. C.; Ray, D. Basic Research Needs: Catalysis for Energy (PNNL-17214). Proceedings from U.S. Department of Energy Workshop, Bethesda, MD, August 6−8, 2007; DOE: Bethesda, MD, 2007; http://www.sc.doe.gov/bes/reports/list.html.
(5) Whipple, D. T.; Kenis, P. J. A. *J. Phys. Chem. Lett.* **2010**, *1*, 3451.
(6) Cole, E. B.; Bocarsly, A. B. In *Carbon Dioxide as Chemical Feedstock*; Aresta, M., Ed.; Wiley-VCH Verlag: Weinheim, 2010; p 291.
(7) Ebbesen, S. D.; Mogensen, M. *J. Power Sources* **2009**, *193*, 349.
(8) Fu, Q. X.; Mabilat, C.; Zahid, M.; Brisse, A.; Gautier, L. *Energy Environ. Sci.* **2010**, *3*, 1382.
(9) Hori, Y. In *Modern Aspects of Electrochemistry*; Vayenas, C. G., White, R. E., Gamboa-Aldeco, M. E., Eds.; Springer: New York, 2008; Vol. *42*, p 89.
(10) Hori, Y.; Wakebe, H.; Tsukamoto, T.; Koga, O. *Electrochim. Acta* **1994**, *39*, 1833.
(11) Noda, H.; Ikeda, S.; Oda, Y.; Imai, K.; Maeda, M.; Ito, K. *Bull. Chem. Soc. Jpn.* **1990**, *63*, 2459.
(12) Augustynski, J.; Kedzierzawski, P.; Jermann, B. *Stud. Surf. Sci. Catal.* **1998**, *114*, 107.
(13) Rosen, B. A.; Salehi-Khojin, A.; Thorson, M. R.; Zhu, W.; Whipple, D. T.; Kenis, P. J. A.; Masel, R. I. *Science* **2011**, *334*, 643.
(14) Stalder, C. J.; Chao, S.; Wrighton, M. S. *J. Am. Chem. Soc.* **1984**, *106*, 3673.
(15) Seshadri, G.; Lin, C.; Bocarsly, A. B. *J. Electroanal. Chem.* **1994**, *372*, 145.
(16) Cole, E. B.; Lakkaraju, P. S.; Rampulla, D. M.; Morris, A. J.; Abelev, E.; Bocarsly, A. B. *J. Am. Chem. Soc.* **2010**, *132*, 11539.
(17) Li, C. W.; Kanan, M. W. *J. Am. Chem. Soc.* **2012**, *134*, 7231.
(18) Hori, Y.; Murata, A.; Kikuchi, K.; Suzuki, S. *J. Chem. Soc., Chem. Commun.* **1987**, 728.
(19) Greenwood, N. N. *Chemistry of the Elements*; Butterworth-Heinemann: Oxford, 1997.
(20) Vela, M. E.; Marchiano, S. L.; Salvarezza, R. C.; Arvia, A. J. *J. Electroanal. Chem.* **1995**, *388*, 133.
(21) Randin, J. P. *Encyclopedia of Electrochemistry of the Elements*; Marcel Dekker: New York, 1976; Vol. *VII*.
(22) Rouya, E.; Cattarin, S.; Reed, M. L.; Kelly, R. G.; Zangari, G. *J. Electrochem. Soc.* **2012**, *159*, K97.
(23) Oesch, U.; Janata, J. *Electrochim. Acta* **1983**, *28*, 1237.
(24) Nishio, K.; Masuda, H. *Angew. Chem., Int. Ed.* **2011**, *50*, 1603.
(25) Kauffman, D. R.; Alfonso, D.; Matranga, C.; Qian, H.; Jin, R. *J. Am. Chem. Soc.* **2012**, *134*, 10237.
(26) Chen, Y.; Kanan, M. W. *J. Am. Chem. Soc.* **2012**, *134*, 1986.
(27) Gileadi, E. *Electrode Kinetics for Chemists, Engineers, and Materials Scientists*; Wiley-VCH: New York, 1993.
(28) Noda, H.; Ikeda, S.; Yamamoto, A.; Einaga, H.; Ito, K. *Bull. Chem. Soc. Jpn.* **1995**, *68*, 1889.